

Thermalization by synchrotron absorption in compact sources: electron and photon distributions

G. Ghisellini¹, F. Haardt² and R. Svensson³

¹ *Osservatorio Astronomico di Brera, V. Bianchi, 46, I-22055 Merate (LC), Italy*

² *Dipartimento di Fisica, Università degli Studi di Milano, V. Celoria 16, I-20133 Milano, Italy*

³ *Stockholm Observatory, Saltsjöbaden, Sweden*

Accepted 1997 December 12; received ***; in original form ***

ABSTRACT

The high energy continuum in Seyfert galaxies and galactic black hole candidates is likely to be produced by a thermal plasma. There are difficulties in understanding what can keep the plasma thermal, especially during fast variations of the emitted flux. Particle–particle collisions are too inefficient in hot and rarefied plasmas, and a faster process is called for. We show that cyclo–synchrotron absorption can be such a process: mildly relativistic electrons thermalize in a few synchrotron cooling times by emitting and absorbing cyclo–synchrotron photons. The resulting equilibrium function is a Maxwellian at low energies, with a high energy tail when Compton cooling is important. Assuming that electrons emit completely self absorbed synchrotron radiation and at the same time Compton scatter their own cyclo–synchrotron radiation and ambient UV photons, we calculate the time dependent behavior of the electron distribution function, and the final radiation spectra. In some cases, the 2–10 keV spectra are found to be dominated by thermal synchrotron self–Compton process rather than by thermal Comptonization of UV disk radiation.

Key words: Galaxies: Radiation mechanisms: miscellaneous — Galaxies: Seyfert — X-Rays: binaries

1 INTRODUCTION

Particle–particle collisions among electrons, and electrons and ions, are rare in rarefied hot plasmas, such as the ones thought to be responsible for the high energy emission in Seyfert galaxies. It is therefore unclear if the plasma in these sources can be described by a thermal, Maxwellian distribution, especially during the fast variations often observed in their X–ray flux and spectrum. On the other hand the OSSE observations of the brightest Seyfert galaxies (i.e. NGC 4151 and IC 4329, see e.g. Zdziarski, Johnson & Magdziarz 1996, Madejski et al. 1995) show the presence of a high energy cut–off, highly indicative of a thermal nature of the underlying plasma. Similar indications are obtained from the sum of 60 combined spectra of 27 Seyfert galaxies (Zdziarski et al. 1995).

In this paper, we propose a new thermalization mechanism, based on the process of synchrotron and cyclotron self–absorption. Electrons embedded in a magnetic field emit and absorb their own cyclo–synchrotron radiation and can exchange energy by exchanging photons. We will show that complete thermalization occurs (in a few cooling times) in sources magnetically dominated and when the radiation is

completely self–absorbed. Increasing the amount of Compton cooling makes the peak of the Maxwellian distribution to shift to lower energies, with the development of a high energy tail.

Using the found equilibrium electron distribution we compute the Comptonization spectra in the framework of the two–phase model of Haardt & Maraschi (1991) and Haardt, Maraschi & Ghisellini (1994). We calculate how the hot magnetized plasma, above a relatively cold accretion disk, reaches a steady state equilibrium distribution through synchrotron self–absorption and by Comptonizing the seed photons coming from the disk. We show that as long as the hot phase is magnetically dominated, the equilibrium temperatures and mean energies of the emitting plasma are in agreement with the existing observations, quite independently of the size of the region. There is however an important difference with respect to a pure thermal scenario, in which particles are assumed to always be in thermal equilibrium. Here, in fact we consider the case of continuous injection of new, energetic electrons, up to some maximum energy $\gamma_{\max} m_e c^2$. This implies that:

1) To reach steady state requires some form of escape of the injected electrons in order to avoid a pile up of cold

electrons. Also reacceleration could occur, but we do not consider this case here.

2) The final distribution is sensitive to the mean energy of the injected electrons, i.e. to γ_{\max} , and to the spectral shape of the injected distribution.

3) We neglect the possible role played by electron–positron pairs created by the produced γ –rays. This could be a self–regulating mechanism to keep γ_{\max} small (see Ghisellini, Haardt & Fabian, 1993). Here we assume a given fixed value of γ_{\max} .

Note that the model proposed here is an hybrid between non–thermal and thermal models, because it assumes a continuous injection of electrons (and not a re–heating), which nevertheless reach a thermal (or quasi–thermal) distribution.

Previous related studies on the subject of synchrotron reabsorption have been made by Ghisellini, Guilbert & Svensson (1988, hereafter GGS88) by Ghisellini & Svensson (1989), and by de Kool, Begelman & Sikora (1989). These studies demonstrated that a quasi–Maxwellian distribution can form at the low energy end of an otherwise power law distribution. In these cases, in fact, electrons were injected at very high energies ($\gamma_{\max} \geq 10^3$) and thin synchrotron emission was the main cooling process. The problem of deriving the equilibrium distribution in the presence of self–Compton losses was briefly discussed by Ghisellini & Svensson (1989).

The present paper differs from previous work because we study a regime where cyclo–synchrotron emission is almost completely self–absorbed, and the main cooling mechanism is due to the Inverse Compton of photons produced in a relatively cold accretion disk.

The structure of the paper is as follows: in Section 2 we describe the main assumptions of the model and the used equations, in Section 3 we describe our results, which are then discussed in Section 4.

2 SET UP OF THE SYSTEM

Assume that in a region of dimension R relativistic electrons are injected at a rate $Q(\gamma)$ [$\text{cm}^{-3} \text{s}^{-1}$] between γ_{\min} and γ_{\max} . A tangled magnetic field B of energy density U_B makes them radiate synchrotron (S) photons. These photons, together with photons produced externally to the region, interact with the electrons by the Inverse Compton (IC) process. If the electron distribution extends to a γ_{\max} of the order of a few, the synchrotron spectrum is completely self absorbed, and the total radiation energy density (U_r) may be dominated by the photons produced externally. We will assume $U_B \gg U_r$. Due to self absorption and the presence of external photons, this does *not* correspond to the prevalence of the synchrotron luminosity over the inverse Compton one.

The electron distribution $N(\gamma, t)$ is the result of the injection, the S and IC losses, and the energy gain due to self absorption (GGS88)

$$\frac{\partial N}{\partial t} = \frac{\partial}{\partial \gamma} \left[(\dot{\gamma}_S + \dot{\gamma}_C)N + H\gamma p \frac{\partial}{\partial \gamma} \left(\frac{N}{\gamma p} \right) \right] + Q - \frac{N}{t_{\text{esc}}}, \quad (1)$$

where the momentum p is measured in units of $m_e c$ and

$\dot{\gamma}_S$ and $\dot{\gamma}_C$ are the cooling rates for synchrotron and Inverse Compton losses, respectively:

$$\dot{\gamma}_S = \frac{4}{3} \frac{\sigma_T c p^2 U_B}{m_e c^2}, \quad (2)$$

$$\dot{\gamma}_C(t) = \frac{4}{3} \frac{\sigma_T c p^2 U_r(t)}{m_e c^2}. \quad (3)$$

Equation (3) assumes that the Compton cooling is in the Thomson regime. The kinetic equation (1) differs from the analogous equation (2) of GGS88 by the inclusion of the Compton loss term $\dot{\gamma}_C$. The factor H is defined below. The last term represents electron escape from the plasma region with the escape time being $t_{\text{esc}} = R/v_{\text{esc}}$. We use $v_{\text{esc}} = c$.

We assume that the radiation energy density U_r is dominated by an external soft photon distribution, and by the ‘hard’ radiation produced by Comptonizing these photons. The soft photons are assumed to arise from the reprocessing of half of the hard radiation by cold matter in the vicinity of the active region as detailed in Haardt & Maraschi (1991). In steady state, all the power injected in the form of relativistic electrons balances the escaping luminosity. Part of the power escapes as kinetic energy flux and part is converted into radiation, mainly at high (UV and X–ray) energies, via IC. The ratio of the two depends upon the ratio of the escape and the IC cooling timescales.

Since the cyclo–synchrotron emission is completely self–absorbed, it is the IC process which is mainly responsible for the radiation losses, even if $U_B \gg U_r$. The Compton process becomes efficient after a time $\approx 2R/c$, which is the timescale required to build up the soft photon radiation field. After this time the radiation energy density can be written as

$$U_r(t) = a \frac{R}{c} (1 + \tau_T) m_e c^2 \int_{\gamma_{\min}}^{\gamma_{\max}} \left[Q(\gamma) - \frac{N(\gamma)}{t_{\text{esc}}} \right] (\gamma - 1) d\gamma, \quad (4)$$

where a is a numerical coefficient (of order unity) which depends on the geometry ($\sim 3/4$ for a sphere and $\sim 1/2$ for a slab). We use $a = 3/4$. The factor $(1 + \tau_T)$ accounts for the enhancement of the photon density due to Thomson scattering with the electrons, the optical depth of which is

$$\tau_T(t) = \sigma_T R \int_1^{\gamma_{\max}} N(\gamma, t) d\gamma. \quad (5a)$$

At equilibrium, the number of injected electrons must be balanced by the number of escaping electrons. In steady state the optical depth becomes

$$\lim_{t \rightarrow \infty} \tau_T(t) = \sigma_T R t_{\text{esc}} \int_{\gamma_{\min}}^{\gamma_{\max}} Q(\gamma) d\gamma. \quad (5b)$$

The factor $H(\gamma, t)$ in equation (1) describes the heating of the electrons and their diffusion in energy. It is defined as

$$H(\gamma, t) = \frac{1}{2m_e^2 c^2} \int_0^{\infty} \frac{J(\nu, t)}{\nu^2} j_s(\nu, \gamma) d\nu, \quad (6)$$

where $j_s(\nu, \gamma)$ is the power spectrum emitted by a single electron through the synchrotron process, and $J(\nu, t)$ is the radiation mean intensity due to the S and IC process, with the former dominating the absorption (and hence the heat-

ing). $J(\nu, t)$ is calculated by

$$J(\nu, t) = \frac{\mu(\nu, t)}{\kappa(\nu, t)} [1 - e^{-R\kappa(\nu, t)}] \quad (7)$$

where $\mu(\nu, t)$ and $\kappa(\nu, t)$ are the emissivity and the absorption coefficient of cyclo-synchrotron radiation, as calculated in GGS88.

Since we are dealing with mildly relativistic electrons, we must specify the cyclo-synchrotron emissivity of the single electron. Most existing expressions are either nonrelativistic or only valid at large harmonics (Petrosian 1981). A simple one parameter phenomenological expression for the cyclo-synchrotron power spectrum is

$$j_s(\nu, \gamma) = \frac{4p^2}{3} \frac{\sigma_T c U_B}{\nu_B} \frac{2}{1+3p^2} \exp\left[\frac{2(1-\nu/\nu_B)}{1+3p^2}\right], \quad (8)$$

where ν_B is the Larmor frequency. This expression (i) has the correct cooling rate, equation (2), when integrated over frequency, (ii) has the correct frequency dependence, $\propto \exp(-2\nu/\nu_B)$, at large harmonics ($\nu \gg \nu_B$) in the non-relativistic limit, (iii) has the correct frequency dependence, at large harmonics in the ultrarelativistic limit, and (iv) the agreement at smaller harmonics, $\nu/\nu_B < 100$, is better than 40% at $\gamma = 2$.

For $\gamma > 2$ we use the usual synchrotron formula averaged over isotropically distributed pitch angles (see, e.g., GGS88).

The kinetic equation (1) can be solved for $N(\gamma, t)$ as a function of $Q(\gamma)$, the magnetic field B , and the size R . Equivalently, besides R , one can specify the injected and the magnetic compactnesses. The total (including rest mass) injected compactness is

$$\ell_{\text{inj}} = \frac{\sigma_T}{m_e c^3} \frac{L_{\text{inj}}}{R}, \quad (9)$$

where

$$L_{\text{inj}} = V m_e c^2 \int_{\gamma_{\text{min}}}^{\gamma_{\text{max}}} Q(\gamma) \gamma d\gamma, \quad (10)$$

and where V is the volume of the region. The magnetic compactness is defined as

$$\ell_B = \frac{\sigma_T}{m_e c^2} R U_B. \quad (11)$$

In the two phase model for Seyfert galaxies, the high energy radiation could be produced by a uniform corona (Haardt & Maraschi 1991) or by localized active regions (possibly highly magnetized; Haardt, Maraschi & Ghisellini, 1994). Assuming the second possibility, the dimensions of each region, or blob, is of the order of a few Schwarzschild radii. (i.e. $R \sim 10^{13}$ cm).

Observations of the high energy continuum and variability in Seyfert galaxies indicate that their compactness is of the order of 1–300 (Done & Fabian, 1989). We then assume that ℓ_{inj} is in these range of values. Our assumption of $U_B \gg U_r$ then also fixes the range of ℓ_B . When escape is not important (i.e., for $\ell_B \gtrsim 1$, see below) we have

$$\frac{U_r}{U_B} \approx \frac{9}{16\pi} \frac{\ell_{\text{inj}}}{\ell_B} \left(1 - \frac{1}{\langle \gamma \rangle}\right) (1 + \tau_T), \quad (12)$$

where $\langle \gamma \rangle$ is the average of γ over $Q(\gamma)$.

The ratio of the cooling time scale, $t_{\text{cool}} = (\gamma - 1)/(\dot{\gamma}_S + \dot{\gamma}_C)$, to the escape time, t_{esc} , is given by

$$\frac{t_{\text{cool}}}{t_{\text{esc}}} \approx \frac{3}{4} \frac{v_{\text{esc}}}{c} \frac{1}{(1 + \gamma)\ell_B(1 + U_r/U_B)}, \quad (13)$$

This is always less than unity for $\ell_B \gtrsim 1$, implying that electrons cool rather than escape for sufficiently large compactnesses. Below we use $\ell_B = 10$ or 30.

Electrons may also thermalize through Coulomb energy exchange (e.g., Stepney 1983, Dermer & Liang 1989, Nayakshin & Melia 1996, Pilla & Shaham 1997). The thermal electron-electron Coulomb energy exchange rate can be approximated with (e.g., Stepney 1983)

$$\dot{\gamma}_{\text{Coul}}(\Theta) \approx \frac{3}{8} \frac{\tau_T c \ln \Lambda}{R \Theta^{1/2} (\pi^{1/2} + \Theta^{1/2})}, \quad (14)$$

where $\ln \Lambda$ is the Coulomb logarithm, typically ≈ 10 –20, and $\Theta \equiv kT/m_e c^2$ is the dimensionless temperature. The thermal average of equation (2) becomes

$$\dot{\gamma}_S(\Theta) \approx (c/R)(4/3)\Theta(1 + 4\Theta)\ell_B. \quad (15)$$

Thermalization by synchrotron selfabsorption dominates when $\dot{\gamma}_S > \dot{\gamma}_{\text{Coul}}$, which gives $\ell_B > (9/32\pi^{1/2})\tau_T \ln \Lambda/\Theta^{3/2}$ for $\Theta < 1$. One sees that the Coulomb process dominates for small temperatures and large τ_T (i.e., large electron densities). From equations (5b), (9), and (10), we find that the Thomson optical depth is given by

$$\tau_T = \frac{3}{4\pi} \frac{v_{\text{esc}}}{c} \frac{\ell_{\text{inj}}}{\langle \gamma \rangle}. \quad (16)$$

Thermalization by synchrotron selfabsorption then dominates for temperatures

$$\Theta > 0.11 \left(\frac{\ln \Lambda}{\langle \gamma \rangle} \frac{\ell_{\text{inj}}}{\ell_B} \right)^{2/3}. \quad (17)$$

3 RESULTS

3.1 Time evolution

Figure 1 shows the evolution of the electron distribution towards the equilibrium configuration. The injected electrons have a Gaussian energy distribution peaking at $\gamma = 10$. The magnetic field has a value $B \simeq 5.5 \times 10^3$ G and the injected power corresponds to $\ell_{\text{inj}} = 1$. The size of the source is $R = 10^{13}$ cm. As can be seen, the equilibrium shape of $\tau(p) \equiv \sigma_T R N(p)$ is reached in a time $\sim 0.1R/c$, about equal to the nonrelativistic cooling time (see eq. 13). With the assumed input parameters, the synchrotron terms (emission, absorption and energy diffusion) in the kinetic equation are dominant over Compton losses. Gains and losses in this case almost perfectly balance. As a result the equilibrium electron distribution is a Maxwellian. Figure 1 also shows that the high energy part of the Maxwellian distribution is formed earlier than the low energy part, due to the higher efficiency of exchanging photons of the high energy electrons. A slower evolution takes place after $0.1(R/c)$, as balance between electron injection and electron escape is achieved on a time scale of a few t_{esc} . Only then have both the shape and the amplitude of $N(p)$ reached their equilibrium values.

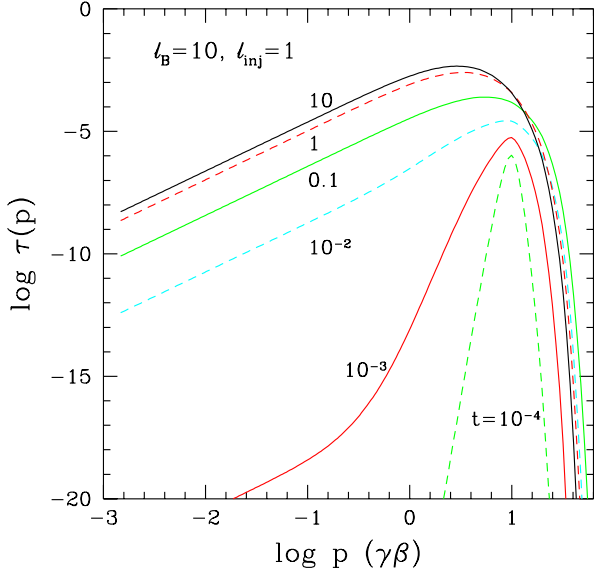


Figure 1. Evolving electron distribution at different times (measured in units of R/c), as labelled. The size of the source is $R = 10^{13}$ cm, $\ell_B = 10$, and $\ell_{inj} = 1$. The injected distribution is a Gaussian centered at $\gamma = 10$.

3.2 Steady equilibrium distributions

The equilibrium distributions for different values of the injected power are shown in Figure 2. The magnetic compactness is set to $\ell_B = 30$, corresponding to $B = 9.6 \times 10^3$ G for $R = 10^{13}$ cm. In all cases, the injected distribution is $Q(\gamma) = Q_0 p/\gamma \exp(-\gamma/\gamma_c)$, where Q_0 is a normalization constant and $\gamma_c = 3.33$. The minimum Lorentz factor is $\gamma_{min} = 1$. The resulting mean injected Lorentz factor is $\langle \gamma \rangle \simeq 4.6$. As long as $\ell_{inj} \ll \ell_B$, the distribution is a quasi-perfect Maxwellian at all energies. This is the result of the quasi-perfect balance between energy gains and losses, as also seen in Fig. 2: Compton losses (not balanced by a corresponding Compton heating term) are a small perturbation. As ℓ_{inj} increases towards values $\simeq \ell_B$, Compton losses start to be relevant, competing with synchrotron processes. At high energies, losses overcome gains, and the electrons diffuse backwards in energy, until the subrelativistic regime is reached. Only in this regime, the increased efficiency of synchrotron gains (relative to losses) halts the systematic backward diffusion in energy, and a Maxwellian can form (see Ghisellini & Svensson 1989). We can evaluate the temperature of this part of $N(\gamma)$ [or, equivalently, of $N(p)$] by fitting a Maxwellian to the low energy part of the distribution, up to energies just above the peak.

The resulting temperatures are plotted in Figure 3 as a function of ℓ_{inj} . As can be seen, for low values of ℓ_{inj} the temperature is quasi-constant, and decreases for ℓ_{inj} greater than 1. Also shown in Figure 3 is the behavior of the “effective temperature” T_{eff} , defined by $[\Theta_{eff} \equiv kT_{eff}/(m_e c^2)]$:

$$16\Theta_{eff}^2 + 4\Theta_{eff} = \frac{4}{3} \langle \gamma^2 - 1 \rangle_N, \quad (18)$$

where the average is over the electron distribution $N(\gamma)$. As expected, for small ℓ_{inj} , T_{eff} is well approximated by T , while

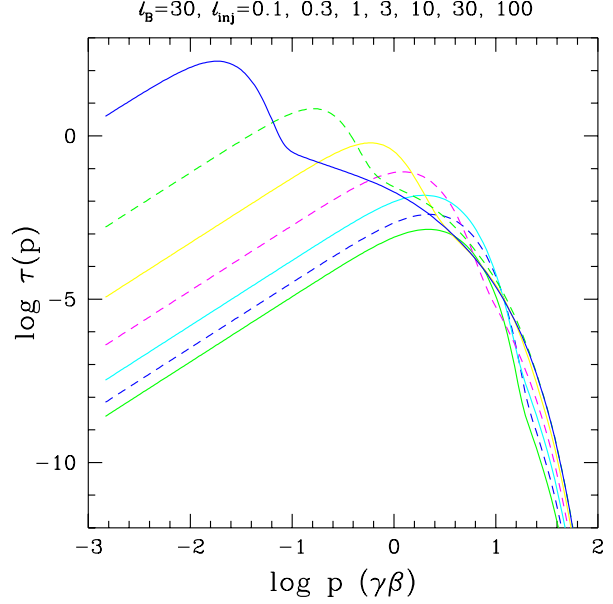


Figure 2. Equilibrium electron distributions for different injected compactnesses (decreasing from top to bottom). $R = 10^{13}$ cm and $\ell_B = 30$ are assumed.

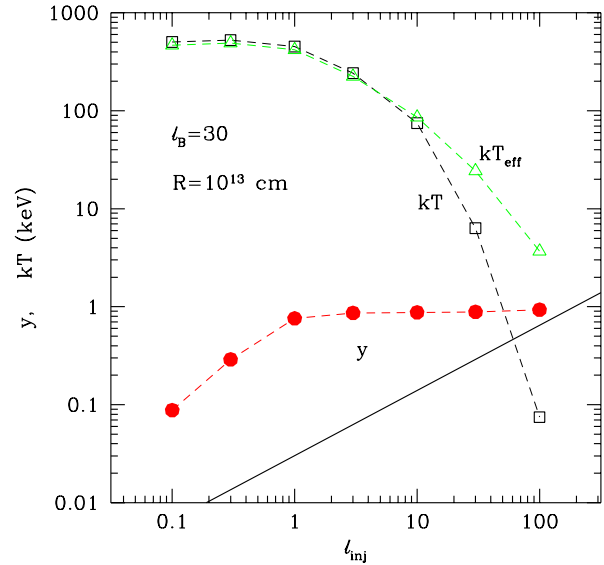


Figure 3. Temperatures and effective temperatures of the distributions shown in Fig. 2. Also shown are the corresponding values of the Comptonization y parameter. Above the solid line, synchrotron self absorption dominates over Coulomb exchange as the thermalization mechanism.

the effective temperature is larger than T for $\ell_{inj} \gtrsim 10$, as a result of the shift of the Maxwellian part to small energies, and the corresponding appearance of the high energy tail.

Along the sequence, the optical depth increases from $\tau_T = 5 \times 10^{-3}$ for $\ell_{inj} = 0.1$ to $\tau_T = 5$ for $\ell_{inj} = 100$, according to equation (16). For our parameters and $\ln \Lambda =$

20, equation (17) becomes $\Theta > 0.03(\ell_{\text{inj}})^{2/3}$, which is plotted as the solid line in Figure 3. One sees that that synchrotron self absorption dominates the thermalization for all cases with ℓ_{inj} smaller than about 60. For the case $\ell_{\text{inj}} = 100$, one cannot neglect Coulomb thermalization.

With the values of Θ_{eff} and τ_{T} , it is of interest to calculate the Compton parameter y defined by

$$y = (\tau_{\text{T}} + \tau_{\text{T}}^2)(16\Theta_{\text{eff}}^2 + 4\Theta_{\text{eff}}), \quad (19)$$

which is also plotted in Figure 3. At equilibrium, τ_{T} is given by equation (16) and Θ_{eff} cannot exceed the value of Θ_{eff} obtained by doing the average in equation (18) over the injected distribution $Q(\gamma)$. This implies that y has a maximum possible value, y_{max} . This limiting value is reached only when radiative cooling is negligible. The actual value of y is then further constrained by the amount of radiative cooling.

For $\ell_{\text{inj}} \geq 1$, $y_{\text{max}} \gg 1$, but the amount of Compton cooling (dominant in this cases) keeps the value of y close to unity. The fact that $y \sim 1$ is to be expected: this value ensures equal power between the Comptonized radiation and the soft seed photon emission.

For $\ell_{\text{inj}} \leq 1$, y_{max} is instead less than unity: Compton cooling is negligible, and the actual value of y is only slightly less than y_{max} , due to synchrotron losses, which, albeit small, are in these cases dominant over Compton losses.

3.3 Spectra

In Figure 4, we show the radiation spectra corresponding to some of the equilibrium electron distributions of Figure 2. Each spectrum consists of several continuum components:

- i) the self-absorbed synchrotron spectrum (S);
- ii) the Comptonized synchrotron spectrum (SSC);
- iii) the thermal soft component (bump);
- iv) the spectrum resulting from Comptonization of the photons from the thermal bump (IC);
- v) the Compton reflection component.

In addition, not shown in the plots, fluorescence line emission from photoionized iron in the accretion disk and absorption features due to partially ionized warm gas along the line of sight are expected to be present in the spectrum.

For each model the values of the compactnesses of the Compton (SSC+IC) component and the synchrotron component are calculated as discussed in §2. In the adopted geometry, neglecting the disk albedo, the compactness corresponding to the soft photon input is $\ell_{\text{soft}} = \ell_{\text{ava}}/(1 + e^{-\tau_{\text{T}}})$, where ℓ_{ava} is the compactness available for radiation production, defined as the difference between the injected and the escaping *kinetic* compactnesses, i.e. subtracting the rest mass energy of the electrons from the total energy.

The temperature of the soft radiation is then calculated assuming black body emission from a region of radius R . The synchrotron and soft component are then Comptonized in a plane parallel slab following the prescriptions described in Haardt (1994). For the synchrotron component we assume a homogeneous source function within the scattering medium, while the thermal soft photon input is localized below the active region, giving rise to anisotropic Compton emission (Haardt 1993). A face-on line of sight is assumed for all the spectra.

The following features may be noticed:

For $\ell_{\text{inj}} \lesssim 1$, the Comptonized spectrum is bumpy, due to the small value of τ_{T} and the large value of Θ . As reported in Figure 3, the y parameter is smaller than unity, making Compton losses relatively unimportant. The synchrotron component, albeit self-absorbed, is more important than the Comptonized power. The luminosity in the thermal “bump” (in the UV) is roughly half of the synchrotron luminosity (in the IR). Therefore, SSC and the IC components have approximately the same luminosity ratio as between the synchrotron and the thermal “bump” luminosities. * Due to the anisotropy Compton effect, *the 2–10 keV band is dominated by the SSC component*, rather than by the IC. This is in contrast to the general view interpreting the high energy emission in Seyfert galaxies as due to Comptonization of thermal bump photons. Here the thermal bump and the X-ray flux are not directly related.

Increasing ℓ_{inj} up to 1, the Compton cooling becomes more important (y approaches 1), making i) the the synchrotron component (and the related SSC) weaker, and ii) the hard X-ray slope flatter.

For $\ell_{\text{inj}} \gtrsim 3$ the Comptonized spectra have the typical IC power law shape, with increasing (steeping) spectral indices as ℓ_{inj} increases. The reason for this steepening even for constant $y = 1$, is explained in detail in Haardt, Maraschi & Ghisellini (1997).

Finally, note that for $\ell_{\text{inj}} \lesssim 3$, the high energy part can be described by an exponential, since the electron distribution is a quasi-perfect Maxwellian in the entire energy range. For $\ell_{\text{inj}} \gtrsim 3$, the electron distribution is more complex (see Fig. 2), resulting in a more complex radiation spectrum above ~ 500 keV.

3.4 Stellar compact sources

The relevant quantities for the synchrotron thermalization process are the injected and the magnetic compactnesses. These parameters are independent of radius, and therefore the process should be largely independent upon the size of the source. However, since $B \propto (\ell_{\text{B}}/R)^{1/2}$ (equation 11), the same value of ℓ_{B} now implies $B = 9.6 \times 10^6$ Gauss. In turn, the increase of the magnetic field implies that the energy range of the electrons emitting optically thick synchrotron radiation is reduced. This affects the synchrotron emission for small values of ℓ_{inj} , which now can have an optically thin component from the most energetic electrons. For illustration, we have repeated our calculations assuming a source size of 10^7 cm, i.e. few Schwarzschild radii for a galactic black hole. For $\ell_{\text{inj}} \gtrsim 1$ the resulting equilibrium electron distributions are almost identical to the $R = 10^{13}$ case, since the synchrotron radiation is completely self-absorbed. For $\ell_{\text{inj}} \lesssim 1$, the results are similar, but the resulting effective

* Note that in Fig. 4 the thermal “bump” appears instead as luminous as the synchrotron component: this is due to the assumed isotropy of the synchrotron emission, while the “bump” emissivity has a $\cos i$ angular pattern, where i is the viewing angle (here, $i = 0^\circ$). Note also that, while the SSC emission is isotropic at all energies, the IC component is not: the emission of the first order scattering in the $i = 0^\circ$ direction is depressed (Haardt 1993). At higher energies, both the IC and the SSC components are isotropic, and here their luminosity ratio has the expected value.

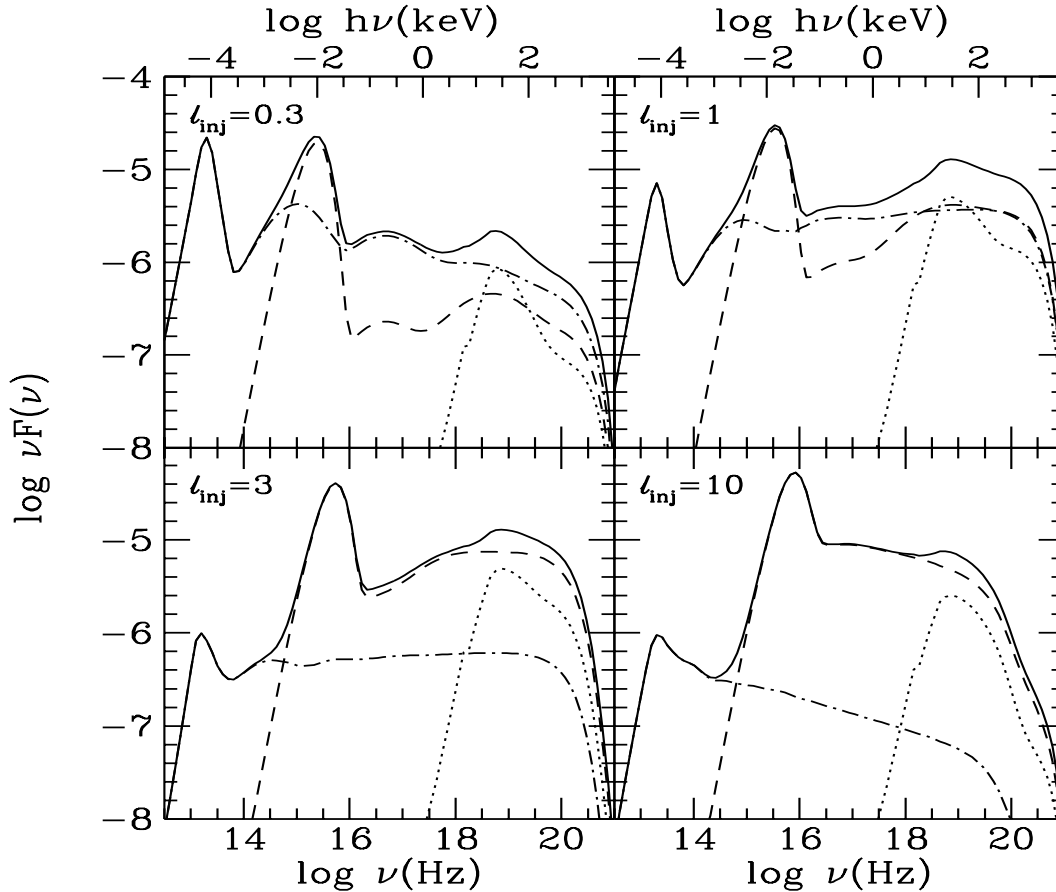


Figure 4. Radiation spectra calculated with the electron distributions shown in Fig. 2. Dashed line: reprocessed thermal bump and IC components. Dash-dotted line: synchrotron and SSC components. Dotted line: Compton reflection component. Solid line: total spectrum.

temperatures are smaller (by a factor 2 for the $\ell_{\text{inj}} = 0.1$ case), due to the presence of a thin synchrotron component.

The computed radiation spectra are shown in Figure 5. They exhibit the same basic features as seen in the extragalactic case (Fig. 4), but with two major differences: i) as expected, the synchrotron emission is more important, with a corresponding more relevant SSC component contributing to the X-ray spectrum for $\ell_{\text{inj}} \lesssim 3$. The increased synchrotron cooling makes the Comptonized components steeper than the corresponding cases in Figure 4; ii) the peak energies of the thermal “bump” and the synchrotron emission are now in the soft X-ray and UV bands, respectively.

4 DISCUSSION AND CONCLUSIONS

We have shown that the exchange of cyclo-synchrotron photons in a self absorbed source is a very efficient thermalization mechanism, especially when the density and temperature of

the plasma prevent the thermalization via particle-particle processes.

In our calculations we assume that the magnetic energy density in the flaring corona dominates over both gas and radiation pressure. This is sensible assumptions in the picture of an active corona. In fact the accretion mechanism is thought to amplify the magnetic field via some sort of dynamo process, and eventually particles in the corona are energized via buoyancy and reconnection of the field lines. Regardless of the largely unknown physics of such processes, it is conceivable that the particles, (and the radiation field they create because of cooling), can not be energetically dominant, as their energy is ultimately drained from the (amplified) magnetic field. Note that this argument is true only if the reconnection timescale is larger than the cooling timescale for a radiating electron, something we have implicitly assumed allowing for steady state particle injection.

We now discuss how the main results of the model change by varying some of the input parameters.

As already mentioned, we have assumed, for all shown cases, an injected electron distribution $Q(\gamma) \propto$

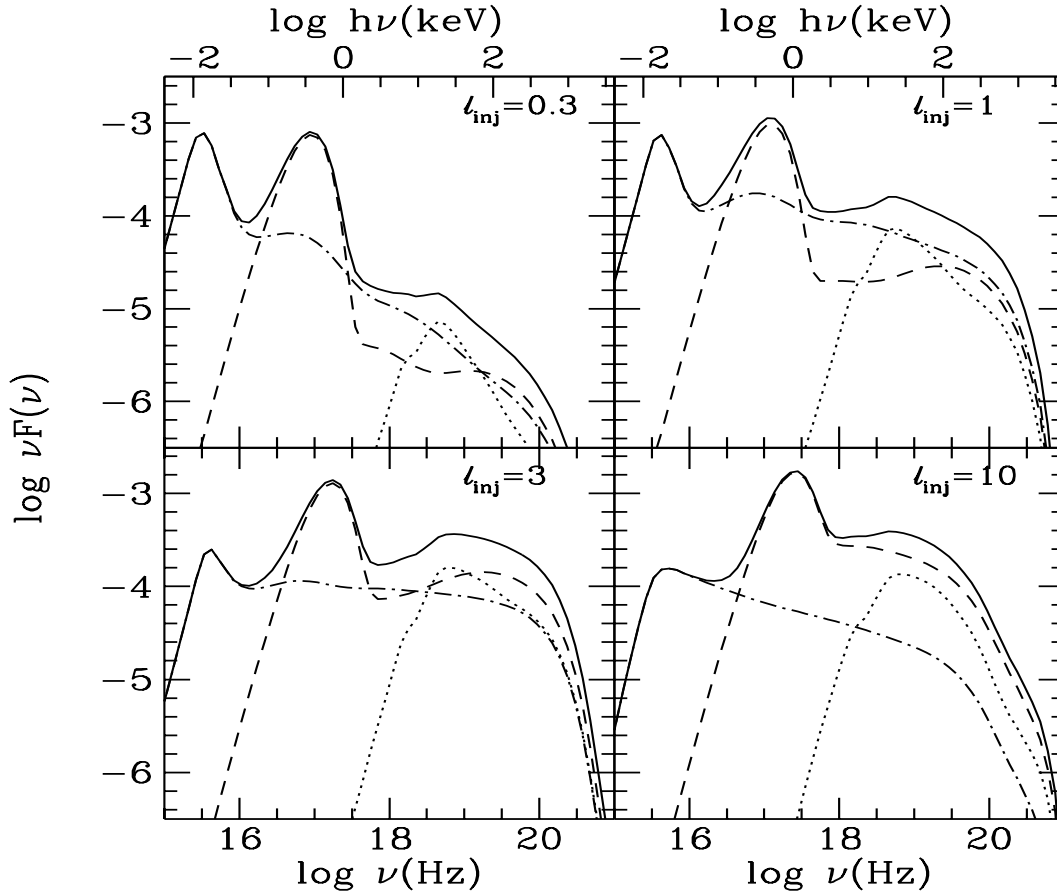


Figure 5. Radiation spectra for the same values of ℓ_B and ℓ_{inj} as in Fig. 4, but for $R = 10^7$ cm. Dashed line: reprocessed thermal bump and IC components. Dash-dotted line: synchrotron and SSC components. Dotted line: Compton reflection component. Solid line: total spectrum.

$\times p/\gamma \exp(-\gamma/\gamma_c)$ with $\gamma_c = 3.33$, resulting in $\langle \gamma \rangle \simeq 4.6$. The emitted radiation spectrum is basically controlled by τ_T , since its value, coupled to the condition $y \simeq 1$, determines the physical conditions in the source. Since $\tau_T \propto \ell_{inj}/\langle \gamma \rangle$ (eq. 16), the assumed *shape* of the injected distribution is not important, as long as different distributions have the same $\langle \gamma \rangle$. Changing ℓ_{inj} and $\langle \gamma \rangle$ by the same factor hence gives rise to the same photon spectrum, provided that the condition $\ell_B \gg \ell_{inj}$ is matched, and that the synchrotron emission is mostly self-absorbed. In other words, the same spectra shown in, e.g., Figure 4, would be obtained for values of ℓ_{inj} different than those indicated if an input distribution with a different $\langle \gamma \rangle$ were used. It is important to note that the value of $\langle \gamma \rangle$ cannot be taken too large, as it changes the fraction of self-absorbed synchrotron radiation. As long as the synchrotron emission is mostly self-absorbed, the spectra obtained for the same value of τ_T and $\ell_{inj}/\langle \gamma \rangle$ are indeed identical. Going to very large $\langle \gamma \rangle$, the conditions of self-absorption breaks down: the electrons cool down mainly because of synchrotron losses, with negligible Comp-

tonization, changing completely the resulting radiation spectrum.

As can be inferred from the shown cases, the value of R is largely unimportant: its value determines the peak frequencies of the synchrotron and bump components, but not the main characteristics of the electron and radiation spectra.

The thermalization process described in this paper is operating whenever energetic electrons and some magnetic field is present, but it becomes of great interest in the study of the high energy spectrum of compact sources when the mean energy of the electrons is less than a few MeV and when the magnetic field is energetically dominant. These conditions ensure that the synchrotron spectrum is completely self-absorbed, and the entire electron distribution is influenced by self-absorption. This also ensures that the synchrotron emission does not overproduce the observed IR (optical) emission observed in radio-quiet AGN (galactic black hole candidates). However, the cyclo-synchrotron process does contribute to the IR (optical) emission, thought to be

mainly due to reprocessing of the primary disk radiation by, e.g., dust.

Since the same electrons contribute also to the X-ray band, simultaneous variability in the IR and X-ray bands should clearly identify this component, allowing the determination of the fraction of synchrotron radiation. Its relative importance decreases by increasing the injected compactness (see Fig. 4).

An important outcome of our calculations concerns the X-ray emission. If the magnetic field is dominant (i.e. its energy density is larger than the radiation energy density) and the Comptonization parameter y is smaller than unity, the scattering of internal cyclo-synchrotron photons is more important than the scattering of the external, “disk” photons. The variability pattern expected in our model is therefore rather complex, since different components can contribute in different bands, and their relative importance depends on the magnetic field dominance. When synchrotron emission is important, the 2–10 keV emission could be only indirectly related to the UV bump photons. Simultaneous UV and X-ray variability (though with different amplitudes) should allow the determination of the importance of the synchrotron and SSC components.

REFERENCES

- Bekefi G. 1966, *Radiation Processes in Plasmas* (New York: Wiley)
- de Kool M., Begelman M. C., Sikora M., 1989, *ApJ*, 337, 66
- Dermer C. D., Liang E. P., 1989, *ApJ*, 339, 512
- Done C., Fabian A. C., 1989, *MNRAS*, 240, 81
- Ghisellini G., Guilbert P., Svensson R., 1988, *ApJ*, 334, L5 (GGS88)
- Ghisellini G., Svensson R., 1989, Physical processes in hot cosmic plasmas, eds. W. Brinkmann, A. C. Fabian & F. Giovannelli, NATO ASI Series, (Kluwer Academic Publishers), p. 395
- Ghisellini G., Haardt F., Fabian A. C., 1993, *MNRAS*, 263, L9
- Haardt F., 1993, *ApJ*, 413, 680
- Haardt F., 1994, PhD thesis, SISSA, Trieste
- Haardt F., Maraschi L., 1991, *ApJ*, 380, L51
- Haardt F., Maraschi L., Ghisellini G., 1994, *ApJ*, 432, L95
- Haardt F., Maraschi L., Ghisellini G., 1997, *ApJ*, 476, 620
- Madejski G. M. et al., 1995, *ApJ*, 438, 672
- Nayakshin S., Melia F., 1996, preprint
- Petrosian V., 1981, *ApJ*, 251, 727.
- Pilla R. P., Shaham J., 1997, *ApJ*, in press
- Stepney S., 1983, *MNRAS*, 202, 467
- Zdziarski A. A., Johnson W. N., Magdziarz P., 1996, *MNRAS*, 283, 193
- Zdziarski A. A., Johnson W. N., Done C., Smith D., McNaron-Brown K., 1995, *ApJ*, 438, L63